Two-Tone Intermodulation in Diode Mixers

STEPHEN A. MAAS, MEMBER, IEEE

Abstract—**This paper explores, experimentally and theoretically, the problem of minimizing second- and third-order intermodulation distortion in diode mixers. A numerical technique is presented which can be used to calculate intermodulation levels with unprecedented accuracy, and it is used to identify circuit and diode parameters which maximize dynamic range. It is shown that intermodulation distortion is minimized by using low diode junction capacitance and series resistance, short-circuit embedding impedances, and high local-oscillator level. It is also shown that certain conditions which may optimize conversion loss, such as image enhancement, may severely exacerbate intermodulation.**

I. Introduction

INTERMODULATION (IM) distortion often defines the upper limit to the signal-handling capability of microwave receiver. It is particularly serious in broad-band receivers designed for communications or spectral surveillance. In such receivers, the mixer is often the major generator of intermodulation distortion, because its signal-handling ability is relatively low. Furthermore, if preamplifier stages are used to achieve a low noise figure, the signal levels applied to the mixer are correspondingly large.

Diode mixers exhibit intermodulation phenomena which have never been explained satisfactorily, and the related problem of selecting diode and circuit parameters to minimize intermodulation has not been investigated. It has been known for many years that the IM output level of a mixer usually, but not always, decreases with an increase in the local oscillator (LO) level, and that nulls in the IM output level sometimes occur at specific values of LO level or dc bias. Beane [1] and Graham and Ehrman [2] explain why some of these phenomena occur, but do not explain why they sometimes do not. Similarly, Lepoff and Cowley [3] and Tou and Chang [4] describe techniques to reduce IM distortion in mixers, but do not address the greater problems of analysis and design for minimal IM. This paper will present analytical techniques which reproduce these phenomena with high accuracy, and will identify diode and circuit parameters which minimize mixer IM.

Many useful techniques for analyzing nonlinear circuits, such as the Volterra series, assume weak nonlinearities and relatively small applied voltages (i.e., a *small-signal, quasi-linear* assumption). Unfortunately, these assumptions are violated by diode mixers, which have a very strong exponential nonlinearity and one signal, the LO, which may be several orders of magnitude larger than the other signals. Even with techniques which do not require a small-signal, quasi-linear assumption, such as that of Ushida and Chua [5], the presence of one signal much larger than the others may introduce numerical problems. One way to circumvent these problems is to treat the pumped diode as a time-varying, weakly nonlinear device. Orloff [6] follows this approach by expanding the junction voltage in a Taylor series, using the LO voltage as the central value, to analyze single-tone IM. Swerdlow [7] applies a time-varying Volterra series to the analysis of a varactor upconverter, assuming a sinusoidal LO current ("current-pumped") waveform. Graham and Ehrman also apply time-varying Volterra series techniques to mixers using lumped circuit elements. Several specialized analyses have been presented [8]–[10] which have various advantages and limitations. The problems with these are that they make implicit or explicit assumptions about the diode's embedding impedances or LO waveforms, do not include junction capacitance or series resistance, or are limited in the order of nonlinearity which can be considered. It will be shown that these factors are critical to mixer IM performance.

The analysis presented here is an extension of existing large-signal/small-signal mixer theory [11], [12]. It requires no assumptions about the LO waveform; any embedding impedance at any mixing or intermodulation frequency can be specified, and both the junction capacitance and conductance nonlinearities are included. By accounting for all important parameters, unprecedented accuracy has been obtained. It is directly applicable to a wide variety of circuits, such as varactor upconverters, subharmonic mixers, and many types of modulators, and the same techniques could be applied to FET mixers. Once the conventional mixer analysis is performed, no further iteration is required. It is efficient enough to be implemented on a small computer such as the IBM PC. Its main limitation is that saturation effects are not included.

II. Theory

Fig. 1 shows the intermediate frequency (IF) spectrum of intermodulation frequencies of greatest concern, up to third order, for two input tones. Only the intermodulation frequencies at the IF are shown, although similar IM voltage and current spectra exist at frequencies above and below each LO harmonic. The variables ω_1 and ω_2 are the desired IF outputs. The diode may have different embedding impedances at each of these frequencies.

Manuscript received July 11, 1986; revised October 29, 1986. This work was supported in part by the U.S. Air Force Space Division under Contract F04701-85-C-0086.

The author is with the Aerospace Corporation, PO Box 92957, Los Angeles, CA 90009.

IEEE Log Number 8612438.

0018-9480/87/0300-0307$01.00 ©1987 IEEE

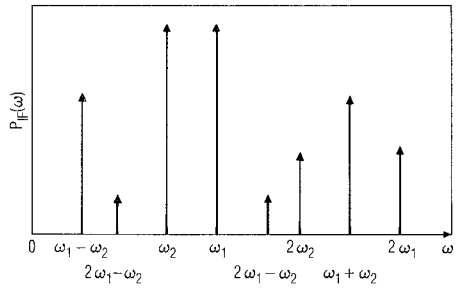

Fig. 1. IF spectrum of the most significant intermodulation components.

The small-signal junction voltage can be treated as a small deviation of the large-signal LO voltage. Hence, the IM current can be found by a Taylor series expansion using the LO voltage as a central "point," and a relatively small number of terms in the series are adequate. The resulting series coefficients are time varying. The general approach is as follows.

1) Perform the large-signal analysis to determine the junction LO voltage and current waveforms.

2) Perform the linear time-varying, small-signal analysis to determine the first-order junction voltages.

3) Use the first-order voltages as excitations to determine the second-order voltages.

4) Use the first- and second-order voltages to determine the third-order voltages.

Steps 1) and 2) are simply the conventional diode mixer analysis. The process could be continued for higher order IM components.

Fig. 2 shows the large-signal equivalent circuit. The diode junction current $I(V_j)$ and capacitive charge $Q(V_j)$ are given by the well-known expressions

$$I_j(V_j) = I_0\left[\exp\left(qV_j/\eta KT\right)-1\right] \cong I_0\exp\left(\delta V_j\right) \quad (1)$$

$$Q(V_j) = -2\phi C_{j0}\left(1-V_j/\phi\right)^{1/2} \quad (2)$$

where I_0 is the diode's reverse saturation current, C_{j0} is the zero-voltage junction capacitance, ϕ is the built-in voltage, q is the electron charge, K is Boltzmann's constant, T is absolute temperature, and η is the ideality factor. Equation (2) implies that the epilayer doping is uniform.

The large-signal analysis of the diode under LO excitation only is performed first via any method which does not involve limiting assumptions (e.g., [13]). It is henceforth assumed that the LO waveforms $I_j(t)$, $V_j(t)$, and $C_j(t) = dQ(V)/dV$, $V = V_j(t)$, are known.

Fig. 3 shows the small-signal equivalent circuit. Here, $i_s(t)$ is the Thevenin equivalent of the RF source, applied directly to the junction, and $v_j(t)$ is the small-signal junction voltage, which includes the IM components and linear terms but not the LO voltage. For two-tone distortion,

$$i_s(t) = I_{s1}\cos\left((m\omega_p+\omega_1)t\right)+I_{s2}\cos\left((m\omega_p+\omega_2)t\right) \quad (3)$$

where ω_p is the LO fundamental frequency. Usually, but not necessarily, $m=1$, implying an upper-sideband RF input. The total junction voltage is $V_j(t)+v_j(t)$. Substituting this into (1) and (2) and expanding in a Taylor series about $V_j(t)$ gives, for the small-signal junction current and charge,

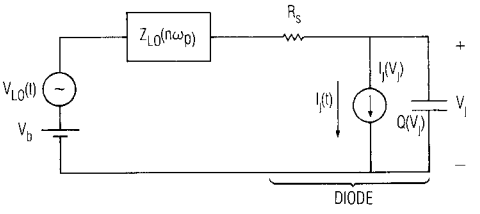

Fig. 2. Large-signal mixer equivalent circuit.

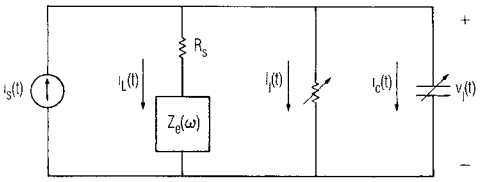

Fig. 3. Small-signal mixer equivalent circuit.

$$i_j(t) = I_j(t)\left[\delta v_j(t)+\delta^2 v_j^2(t)/2+\delta^3 v_j^3(t)/6+\cdots\right] \quad (4)$$

$$q_j(t) = C_j(t)\left[2\left(\phi-V_j(t)\right)v_j(t)+\left(\phi-V_j(t)\right)^{-1}v_j^2(t)/4 + \left(\phi-V_j(t)\right)^{-2}v_j^3(t)/8+\cdots\right]. \quad (5)$$

Equations (4) and (5) can be expressed more generally as

$$i_j(t) = g_1(t)v_j(t)+g_2(t)v_j^2(t)+g_3(t)v_j^3(t)+\cdots \quad (6)$$

$$q_j(t) = c_1(t)v_j(t)+c_2(t)v_j^2(t)+c_3(t)v_j^3(t)+\cdots. \quad (7)$$

Limiting consideration to third-order IM components,

$$v_j(t) = v_1(t)+v_2(t)+v_3(t) \quad (8)$$

$$v_j^2(t) = v_1^2(t)+2v_1(t)v_2(t) \quad (9)$$

$$v_j^3(t) = v_1^3(t) \quad (10)$$

where $v_n(t)$ is the nth-order IM voltage, the sum of the frequencies of any n first-order junction voltages. The differential equation describing Fig. 3 is

$$\frac{dq_j(t)}{dt}+i_j(t)+i_L(t) = i_s(t). \quad (11)$$

Substituting (6)–(10) into (11) and separating gives the equations for first-, second-, and third-order products

$$\frac{d}{dt}\left(c_1(t)v_1(t)\right)+g_1(t)v_1(t)+i_{L1}(t) = i_s(t) \quad (12)$$

$$\frac{d}{dt}\left(c_1(t)v_2(t)+c_2(t)v_1^2(t)\right)+g_1(t)v_2(t) + g_2(t)v_1^2(t)+i_{L2}(t) = 0 \quad (13)$$

$$\frac{d}{dt}\left(c_1(t)v_3(t)+2c_2(t)v_1(t)v_2(t)+c_3v_1^3(t)\right) + g_1(t)v_3(t)+2g_2(t)v_1(t)v_2(t) + g_3(t)v_1^3(t)+i_{L3}(t) = 0 \quad (14)$$

where I_{L1}, I_{L2}, and I_{L3} are the first-, second-, and third-order load currents, respectively.

Parts (a), (b), and (c) of Fig. 4 show the first-, second-, and third-order equivalent circuits representing (12), (13), and (14), respectively. Fig. 4(a) is the small-signal linear equivalent circuit. The voltage components of $v_1(t)$ resulting from the two excitation tones can be found in the conventional manner. These are used to find the excitation currents, the sources in Fig. 4(b), for the second-order IM components. (These sources are in fact the short-circuit junction IM currents.) Given those currents, Fig. 4(b) is a linear circuit, so $v_2(t)$ and $i_{L2}(t)$ can be found by conversion matrix analysis in the same manner as $i_{L1}(t)$ and $v_1(t)$. The third-order IM products are found analogously through the circuit in Fig. 4(c).

The small-signal linear mixer analysis gives $v_1(t)$:

$$v_1(t) = \frac{1}{2} \sum_{m=-\infty}^{\infty} \sum_{\substack{q=-2 \\ q\neq 0}}^{2} V_{m,q} \exp\left[j(m\omega_p + \omega_q)t\right] \quad (15)$$

so

$$v_1^2(t) = \frac{1}{4} \sum_{\substack{m \\ =-\infty}}^{\infty} \sum_{n} \sum_{\substack{q \\ =-2 \\ q,r\neq 0}} \sum_{r}^{2} V_{m,q} V_{n,r} \cdot \exp\left\{ j\left[(m+n)\omega_p + \omega_q + \omega_r\right]t \right\}. \quad (16)$$

The second-order terms of most interest are those at $k\omega_p + \omega_1 - \omega_2$ and $k\omega_p + 2\omega_1$. These are the second-order IM frequencies most likely to cause interference, and are needed to find the third-order IM components. They will be designated by a and b subscripts, respectively. Then

$$v_{1a}^2(t) = \frac{1}{2} \sum_{\substack{m \\ =-\infty}}^{\infty} \sum_{n} V_{m,1} V_{n,-2} \cdot \exp\left\{ j\left[(m+n)\omega_p + \omega_1 - \omega_2\right]t \right\} \quad (17)$$

$$v_{1b}^2(t) = \frac{1}{4} \sum_{\substack{m \\ =-\infty}}^{\infty} \sum_{n} V_{m,1} V_{n,1} \cdot \exp\left\{ j\left[(m+n)\omega_p + 2\omega_1\right]t \right\}. \quad (18)$$

Equation (17) has a coefficient of 1/2, instead of 1/4, because there are two identical terms in the summation over q, r in (16) for this frequency component. This situation arises repeatedly in the following equations.

The Taylor series coefficients can be expressed by their Fourier series' as

$$g_2(t) = \frac{\delta^2}{2} I_j(t) = \frac{\delta^2}{2} \sum_{l=-\infty}^{\infty} I_l \exp(jl\omega_p t) \quad (19)$$

$$c_2(t) = \frac{C_j(t)}{4(\phi - V_j(t))} = \sum_{l=-\infty}^{\infty} C_{2,l} \exp(jl\omega_p t). \quad (20)$$

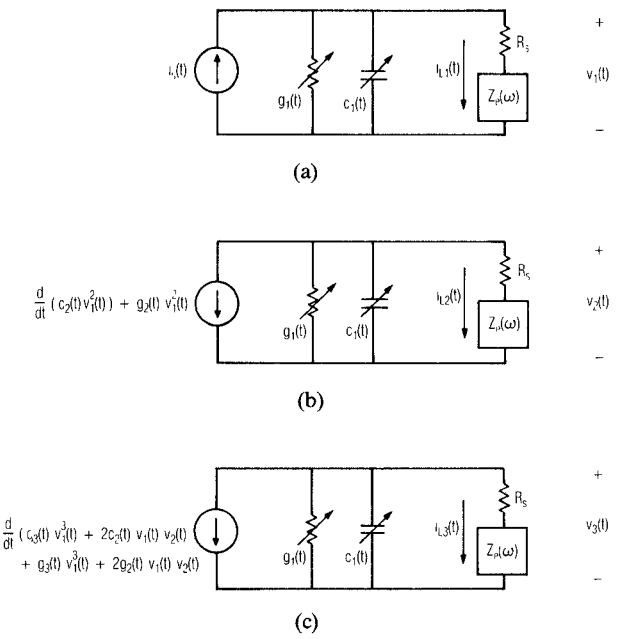

Fig. 4. Small-signal equivalent circuits for (a) first order, (b) second order, and (c) third-order IM products.

Using (17)–(20), Fig. 4(a), and (13), the excitation current components are

$$i_{2a}(t) = \frac{1}{2} \sum_{\substack{l \\ =-\infty}}^{\infty} \sum_{m} \sum_{n} V_{m,1} V_{n,-2} \cdot \left(\frac{\delta^2}{2} I_l + C_{2,l} j\left[(l+m+n)\omega_p + \omega_1 - \omega_2\right] \right) \cdot \exp\left\{ j\left[(l+m+n)\omega_p + \omega_1 - \omega_2\right]t \right\} \quad (21)$$

$$i_{2b}(t) = \frac{1}{4} \sum_{\substack{l \\ =-\infty}}^{\infty} \sum_{m} \sum_{n} V_{m,1} V_{n,1} \left(\frac{\delta^2}{2} I_l + C_{2,l} j\left[(l+m+n)\omega_p + 2\omega_1\right] \right) \exp\left\{ j\left[(l+m+n)\omega_p + 2\omega_1\right]t \right\}. \quad (22)$$

Here, $i_{2a}(t)$ and $i_{2b}(t)$ are of the form

$$i_{2a}(t) = \frac{1}{2} \sum_{k=-\infty}^{\infty} I_{k,2a} \exp\left[j(k\omega_p + \omega_1 - \omega_2)t\right] \quad (23)$$

$$i_{2b}(t) = \frac{1}{2} \sum_{k=-\infty}^{\infty} I_{k,2b} \exp\left[j(k\omega_p + 2\omega_1)t\right]. \quad (24)$$

Equating terms at the same frequency in (23)/(21) and (24)/(22), one obtains

$$I_{k,2a} = \frac{1}{2} \sum_{\substack{l \\ =-\infty \\ l+m+n=k}}^{\infty} \sum_{m} \sum_{n} V_{m,1} V_{n,-2} \cdot \left(\frac{\delta^2}{2} I_l + C_{2,l} j(k\omega_p + \omega_1 - \omega_2) \right) \quad (25)$$

and

$$I_{k,2b}=\frac{1}{2}\sum_{\substack{l\\ l+m+n=k}}\sum_{\substack{m=-\infty}}^{\infty}\sum_{n} V_{m,1}V_{n,1}\left(\frac{\delta^2}{2}I_l+C_{2,l}j(k\omega_p+2\omega_1)\right). \tag{26}$$

The value $k=l+m+n$ must be limited to some range $(-K, K)$; then (25) and (26) can be expressed as column vectors of the form

$$\boldsymbol{I}_{2a}=(I_{-K,2a}\ I_{-K+1,2a}\cdots I_{-1,2a}\ I_{0,2a}\ I_{1,2a}\cdots I_{K,2a})^T \tag{27}$$

and similarly for $\boldsymbol{I}_{2b}$.

The vectors of output IM currents, $\boldsymbol{I}_{12a}$ and $\boldsymbol{I}_{12b}$, are found from a straightforward conversion matrix analysis of Fig. 4b:

$$\boldsymbol{I}_{L2a}=-\left(\mathbf{1}+\boldsymbol{Y}_j(\boldsymbol{Z}_{e2a}+R_s\mathbf{1})\right)^{-1}\boldsymbol{I}_{2a} \tag{28}$$

$$\boldsymbol{I}_{L2b}=-\left(\mathbf{1}+\boldsymbol{Y}_j(\boldsymbol{Z}_{e2b}+R_s\mathbf{1})\right)^{-1}\boldsymbol{I}_{2b}. \tag{29}$$

$\boldsymbol{Y}_j$ is the conversion matrix for the pumped diode junction [12]. $\boldsymbol{Z}_{e2a}$ and $\boldsymbol{Z}_{e2b}$ are the $2K+1\times 2K+1$ diagonal matrices of embedding impedances at the IM frequencies, with the impedances at $K\omega_p+\omega_1-\omega_2$ and $K\omega_p+2\omega_1$ at the top left corners, respectively. R_s is the diode series resistance. The second-order junction voltages are

$$\boldsymbol{V}_{2a}=(\boldsymbol{Z}_{e2a}+R_s\mathbf{1})\boldsymbol{I}_{L2a} \tag{30}$$

$$\boldsymbol{V}_{2b}=(\boldsymbol{Z}_{e2b}+R_s\mathbf{1})\boldsymbol{I}_{L2a} \tag{31}$$

and the second-order IM output powers at the IM frequencies near the kth LO harmonic are

$$P_{k,2a}=0.5|I_{k,L2a}|^2\,\mathrm{Re}\{Z_{e2a,k}\} \tag{32}$$

$$P_{k,2b}=0.5|I_{k,L2b}|^2\,\mathrm{Re}\{Z_{e2b,k}\}. \tag{33}$$

The third-order IM components are found analogously via (14) and Fig. 4(c). The IM component of greatest interest is that at $2\omega_1-\omega_2$ (or $2\omega_2-\omega_1$, which is derived identically), since it usually cannot be rejected by filters. The $v_1(t)v_2(t)$ term in (14) has two components which generate $2\omega_1-\omega_2$: $v_1(t)$ at ω_1 mixing with $v_{2a}(t)$ at $\omega_1-\omega_2$, and $v_1(t)$ at $-\omega_2$ mixing with $v_{2b}(t)$ at $2\omega_1$. The components of $v_1^3(t)$ and $v_1(t)v_2(t)$ at these frequencies are

$$v_1^3(t)=\frac{3}{8}\sum_{\substack{m=-\infty}}^{\infty}\sum_{n}\sum_{p} V_{m,1}V_{n,1}V_{p,-2}\cdot\exp\left\{j\left[(m+n+p)\omega_p+2\omega_1-\omega_2\right]t\right\}. \tag{34}$$

Again, the coefficient is 3/8 instead of 1/8 because there are three identical terms in the q, r summation:

$$v_1(t)v_{2a}(t)=\frac{1}{4}\sum_{\substack{m=-\infty}}^{\infty}\sum_{n} V_{m,2a}V_{n,1}\cdot\exp\left\{j\left[(m+n)\omega_p+2\omega_1-\omega_2\right]t\right\} \tag{35}$$

and

$$v_1(t)v_{2b}(t)=\frac{1}{4}\sum_{\substack{m=-\infty}}^{\infty}\sum_{n} V_{m,2b}V_{n,-2}\cdot\exp\left\{j\left[(m+n)\omega_p+2\omega_1-\omega_2\right]t\right\}. \tag{36}$$

The IM coefficients $c_3(t)$ and $g_3(t)$ are

$$c_3(t)=\sum_{l=-\infty}^{\infty}C_{3,l}\exp(jl\omega_p t) \tag{37}$$

$$g_3(t)=\frac{\delta^3}{6}\sum_{l=-\infty}^{\infty}I_l\exp(jl\omega_p t). \tag{38}$$

An analogous treatment for (14) gives the components of the third-order source and IM output current vectors:

$$\begin{aligned}I_{k,3}=\frac{1}{4}&\sum_{\substack{l+m+n+p=k}}\sum_{\substack{l\\ m=-\infty}}^{\infty}\sum_{n}\sum_{p} V_{m,1}V_{n,1}V_{p,-2}\cdot\left(\frac{\delta^3}{2}I_l+3C_{3,l}j\left[k\omega_p+2\omega_1-\omega_2\right]\right)\\ &+\sum_{\substack{l+m+n=k}}\sum_{\substack{l\\ m=-\infty}}^{\infty}\sum_{n}(V_{m,2a}V_{n,1}+V_{m,2b}V_{n,-2})\cdot\left(\frac{\delta^2}{2}I_l+C_{2l}j\left[k\omega_p+2\omega_1-\omega_2\right]\right)\end{aligned} \tag{39}$$

$$\boldsymbol{I}_{L3}=\left(\mathbf{1}+\boldsymbol{Y}_j(\boldsymbol{Z}_{e3}+R_s\mathbf{1})^{-1}\boldsymbol{I}_3\right. \tag{40}$$

where $\boldsymbol{Z}_{e3}$ is the embedding impedance matrix at the third-order mixing frequencies and $\boldsymbol{I}_3$ is the third-order source-current column vector. The output IM power at $k\omega_p+2\omega_1-\omega_2$ is

$$P_{k,3}=0.5|I_{k,L3}|^2\,\mathrm{Re}\{Z_{e3,k}\}. \tag{41}$$

III. Implementation

The Turbo–Pascal [14] program DIODEMX listed in [12] was modified to include the IM calculations [15]. DIODEMX calculates the LO voltage, current, and capacitance waveforms $V_j(t)$, $I_j(t)$, and $C_j(t)$ via a harmonic balance technique. It then forms conversion matrices for the junction and finds the first-order junction voltages $V_{m,\pm 1}$ and $V_{n,\pm 2}$. It also supplies the matrix $\boldsymbol{Y}_j$ for (28), (29), and (40). The evaluation of the multiple summations and the determination of the IM output powers are then performed by a single new subroutine. Some economies in execution time are obtained by recognizing that many of the terms in the multiple summations are identical, and need not be evaluated repeatedly. Considering 12 LO harmonics in I_l, $C_{2,l}$, and $C_{3,l}$, and nine mixing frequencies in the conversion matrices and in $V_{m,\pm 1}$ and $V_{n,\pm 2}$, execution of the IM subroutine requires 49 seconds using an IBM PC with an 8087 math coprocessor. Execution time is

approximately half this value with an 80286-based microcomputer and 80287 numeric coprocessor.

The calculations can be simplified by the assumptions that the two input tones are closely spaced in frequency and that the IM outputs are within the IF passband. Under this assumption, $V_{m,\pm 1} = V_{m,\pm 2}$, $Z_{e3} = Z_{e2} = Z_{e1}$, and (28), (29), and (40) are identical, and a large block of impedance data need not be entered. The validity of this assumption may be questionable in certain cases only for either the $2\omega_1$ or the $\omega_1 - \omega_2$ component, one of which may be well separated from the other. In most cases, the results are of acceptable accuracy even if the assumptions are not strictly valid. In situations where this approximation is not acceptable, one can enter the IF load impedances for these components individually.

IV. Results

The theory was verified experimentally with a single-ended mixer operating at approximately 10.5 GHz with an IF near 50 MHz. The sole purpose of the mixer was to verify the theory, not to achieve any performance goals; it was designed primarily to have predictable embedding impedances at as many LO harmonics and mixing frequencies as possible. The mixer consists of a diode mounted at the end of a 50-Ω microstrip line, with a 10 pF dc/IF blocking capacitor at the input and a decoupling circuit for dc bias and the IF output. LO and RF were applied through the input port via a directional coupler. Bias was applied through a bias tee in the IF circuit. The mixer was realized in microstrip on a 0.025-in alumina substrate.

The diode was silicon Schottky-barrier beam-lead device (Alpha model no. DMJ6777). Its parameters were $R_s = 6.0$ Ω, $C_{j0} = 0.15$ pF, $\phi = 0.7$ V, $\eta = 1.19$, and $I_0 = 5.0 \times 10^{-12}$ A, determined by direct measurement of its C/V and I/V characteristics. The beam-lead overlay capacitance plus the calculated microstrip open-end capacitance was 0.10 pF. This capacitance in parallel with the 50-Ω source comprised the embedding network.

Fig. 5 shows the measured and calculated conversion loss and the third-order IM output level for −20-dBm input, with zero dc bias. The calculations include the effect of an estimated 0.5-dB input loss. Fig. 6 shows the two second-order IM output levels under the same conditions. Fig. 7 shows the measured and calculated dependence of conversion loss and IM upon dc bias voltage at a fixed LO level of 0 dBm. The agreement over a wide LO power range is remarkably good; in particular, the nulls in IM level at specific values of LO power and bias are faithfully reproduced.

Other mixer and diode parameters were examined to identify those which most strongly affect mixer IM performance. A set of baseline diode and circuit parameters was defined, and certain of these were varied while the rest were held fixed. The baseline parameter values were $C_{j0} = 0.15$ pF, $R_s = 9.0$ Ω, $\eta = 1.30$, $\phi = 0.6$ V, and $I_0 = 2.6 \times 10^{-9}$A. The embedding impedances were zero at the image frequency, LO harmonics, and all high-order mixing fre-

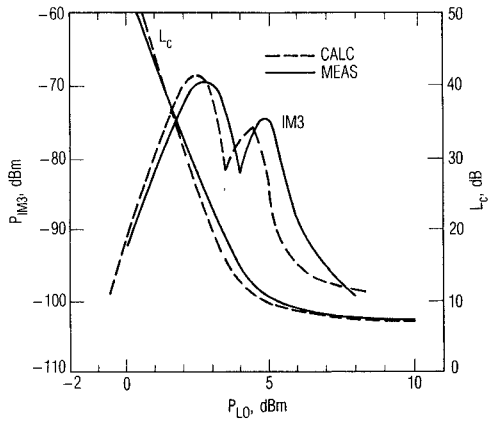

Fig. 5. Measured (solid line) and calculated (dashed line) conversion loss and third-order IM output levels for −20-dBm RF input per tone.

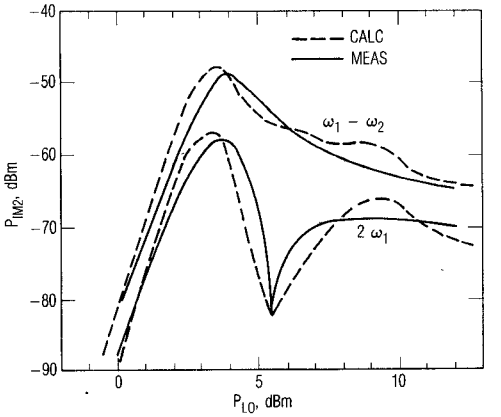

Fig. 6. Measured (solid line) and calculated (dashed line) second-order IM output levels for −20-dBm RF input per tone.

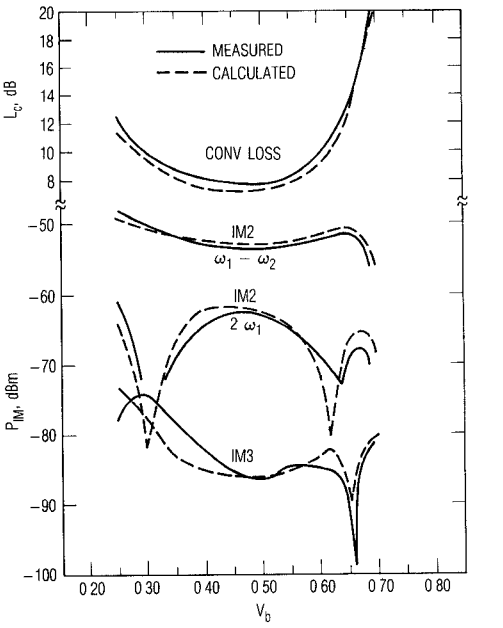

Fig. 7. Measured (solid line) and calculated (dashed line) conversion loss and IM levels as a function of dc bias voltage. LO power is 0 dBm.

quencies. The LO fundamental source impedance was $50+j0\ \Omega$. In order to eliminate uncertainties due to source/load VSWR, all data were tabulated for simultaneously conjugate-matched RF and IF ports. This approach has the disadvantage that the conversion loss optimum often occurs at very low LO levels, sometimes with impractically high source/load impedances, and if the mixer is conditionally stable, a simultaneous conjugate match is impossible. For the most important cases of high LO level (i.e., $\gtrsim 3$ dBm), however, impedances are invariably reasonable and the mixer is stable. The RF frequencies were 10.54 and 10.56 GHz and the LO frequency was 10.50 GHz. The RF input level was -20 dBm per tone.

Fig. 8 shows the calculated conversion loss and third-order IM level for short-circuit and open-circuit high-order small-signal and LO embedding impedances. Also shown are the same data with 50-Ω LO embedding impedances. Fig. 9 shows the second-order IM levels under the same conditions. The drop in IM level with increased LO power shown in Figs. 5–9 is contrary to intuition, because the LO voltage traverses a progressively more strongly nonlinear range of the I/V and C/V characteristics. The reason is that at high LO levels the junction operates more like a switch than a continuous nonlinearity, and IM current is generated only during the transition between reverse bias and hard forward conduction. This transition becomes shorter as LO power is increased. Similarly, operating the mixer in any way that reduces the length of this transition will reduce intermodulation levels.

The effect of different embedding impedances on the IM level can be related to the interplay of two phenomena. The matrix term in (40) is small for large values of $\boldsymbol{Z}_{e3}$, indicating that IM output current should be small. However, the magnitudes of the junction voltage components $V_{m,q}$ are relatively large and many may be significant, increasing the magnitudes of the components of the current vector $\boldsymbol{I}_3$ in (39). The net effect is that the IM levels for short-circuit and open-circuit embedding impedances are comparable at low LO levels, but at high levels the IM output power rises. Furthermore, if the LO source impedance is high, C_j must discharge through a high impedance during the negative-going half of the LO cycle. This slows the transition between conduction and turn-off, and consequently increases IM levels. Hence, it appears that the best possible IM performance is achieved with short-circuit embedding impedances and heavy LO pumping.

The variation in IM level with LO level in many cases has multiple nulls. This phenomenon is a manifestation of the fact that the excitation currents in parts (b) and (c) of Fig. 4 are not a single sinusoid, but a spectrum of components, related in phase, each downconverted to the same IF. These IF current components experience phase cancellation at certain LO levels. This phenomenon is sensitive in some degree to virtually all mixer and diode parameters, so it is questionable whether it can be used in practice to reduce IM levels significantly.

Fig. 10 shows the effect of image enhancement upon IM level, noise temperature, and conversion loss by varying

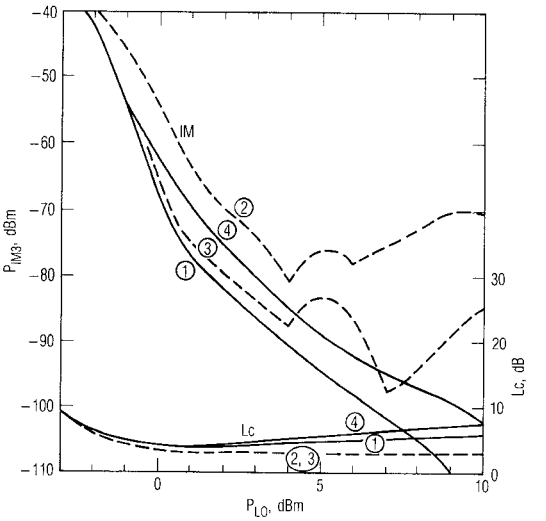

Fig. 8. Conjugate match conversion loss and third-order IM for different sets of high-order LO and RF embedding impedances: (1) Z_e, Z_{LO} short-circuit; (2) Z_e, Z_{LO} open-circuit; (3) Z_e open-circuit, $Z_{LO} = 50+j0$; (4) Z_e short circuit, $Z_{LO} = 50+j0$. The LO fundamental embedding impedance is $50+j0$. Conversion loss for (2) and (3) are virtually identical.

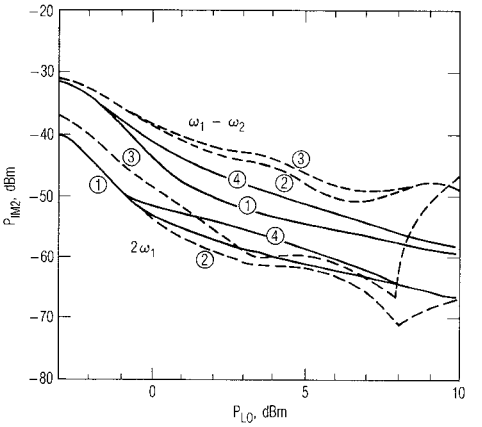

Fig. 9. Second-order IM output levels for the same conditions as in Fig. 8.

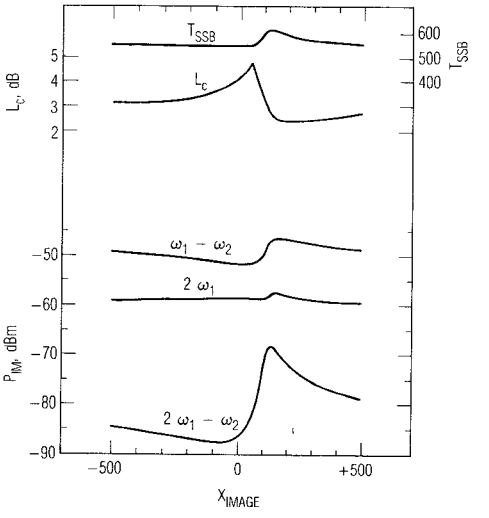

Fig. 10. Conjugate-match conversion loss, IM levels, and noise temperature as a function of image termination reactance. All LO and small-signal high-order embedding impedances, except for the image, are zero. $P_{LO} = 3$ dBm, $V_b = 0$.

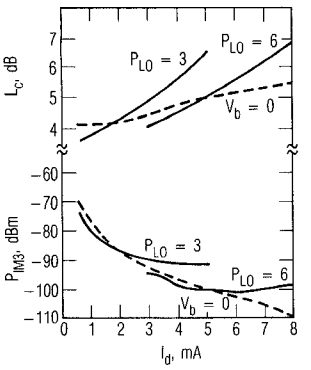

Fig. 11. Conversion loss and IM level versus dc diode current for fixed LO power and fixed bias voltage conditions.

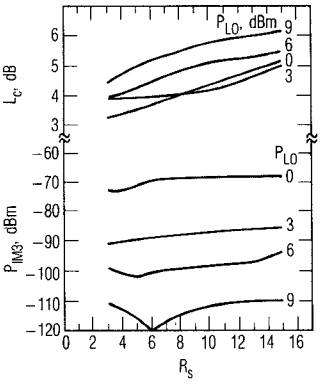

Fig. 12. Conversion loss and IM level dependence on series resistance.

the value of a purely reactive image termination. The termination which gives minimum conversion loss results in a remarkably high noise temperature, a modest rise in second-order IM level, and an enormous rise in third-order IM. Part of the reason for this rise is the high value of IF load impedance, 600 Ω, necessary to achieve a simultaneous conjugate match at this value of image reactance. It is clear that the best overall performance for this mixer is achieved with a capacitive termination or a short circuit. This phenomenon—low conversion loss accompanied by high noise—is often observed experimentally. It is sobering to note that it may also be accompanied by very poor IM performance.

In Fig. 11, L_c and the IM level are graphed as functions of dc diode current, for fixed bias with the LO level varied, and two fixed LO levels with the dc bias varied from −0.2 to 0.3 V. The curves for fixed P_{LO} and fixed V_b overlap over wide ranges, but the conversion loss is somewhat better for fixed bias. This remarkable result is due to the fact that the transition regions in the LO waveform vary nearly identically as either bias voltage or LO level is increased. L_c, however, is affected most strongly by the shape of the conductance waveform, which varies differently with bias and LO level. These results imply that in some cases dc bias can be traded for LO power in order to minimize IM levels.

Figs. 12 and 13 show the dependence of third-order IM upon diode series resistance and junction capacitance, respectively, for three LO power levels. In all cases, the

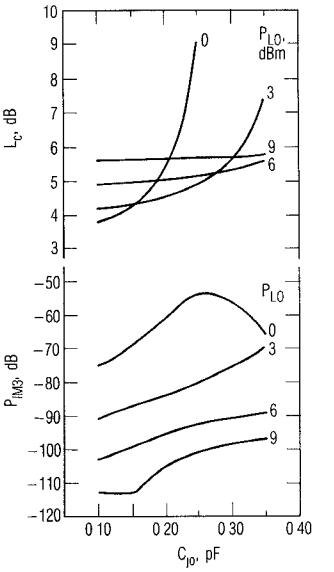

Fig. 13. Conversion loss and IM level dependence on zero-voltage junction capacitance.

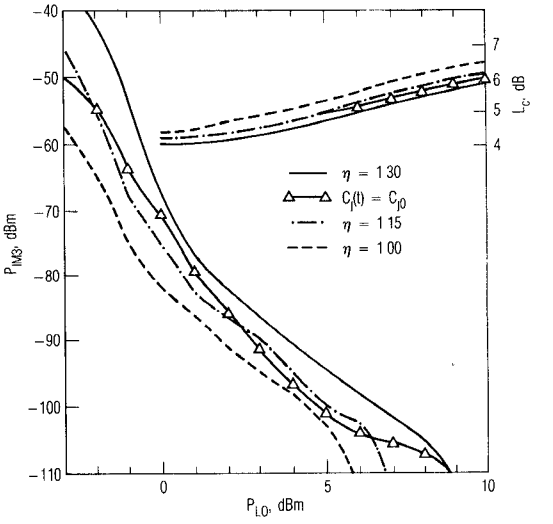

Fig. 14. Conversion loss and IM level dependence on ϕ and η.

dependence on LO level is stronger than that on diode parameters. Nevertheless, at the high end of the LO range, a low series resistance and low junction capacitance are clearly advantageous. C_{j0} has a remarkably strong effect on IM level, even though its nonlinearity is relatively weak and it generates little IM current by itself. Its significance comes from its effect on the LO waveform: a low junction capacitance discharges rapidly, allowing the junction voltage to drop through the conduction/nonconduction transition rapidly. Generally, low R_s results in low IM. The rise in IM level for very low R_s at high LO levels may be related to the fact that this mixer is conditionally stable at some LO levels for $R_s < 4\Omega$. Most real mixers would probably have enough loss in their embedding networks to prevent instability, so this phenomenon might not be observed in practice. Minimizing R_s is consistent with the need to minimize all embedding impedances.

Fig. 14 shows the dependence of IM level upon ϕ and η.

Setting ϕ to a large value removes the variation of junction capacitance, and therefore approximates a Mott diode. This change reduces IM level slightly, probably by minimizing the peak value of C_j. Minimizing η also minimizes IM levels. The drop in conversion loss with increase in η may be surprising. For a conjugate-matched diode, conversion loss rises with LO power above the optimum LO level, in this case 0 dBm, because the junction conductance pulse is longer than optimum. Low η gives a longer conductance pulse, for a given LO level, than does high η. Therefore, the mixer achieves a given value of conversion loss at a lower LO level for low η than high. The noise temperature is, as one might expect, significantly lower for low η than for high η.

V. Conclusions

This paper has shown that intermodulation in diode mixers can be predicted with high accuracy. Intermodulation is most strongly related to the speed of the diode's transition between hard conduction and nonconduction, the magnitudes of its junction voltage IM components, and the magnitude of its embedding impedances. The results indicate that the most significant parameter affecting mixer IM performance is LO level. However, high LO level alone is not sufficient to achieve low intermodulation; it is necessary to optimize all mixer diode and circuit parameters. The best IM performance is obtained by using a high-quality diode with low junction capacitance and series resistance. Embedding impedances should be short circuits, and dc bias should be used. Image enhancement must be used with care.

Acknowledgment

The author wishes to thank R. M. Gowin for assistance with the fabrication of the mixers, W. A. Garber for measuring the diode C/V characteristic, and M. McColl, W. A. Johnson, and F. L. Vernon for reading and commenting on this paper.

References

[1] E. F. Beane, "Prediction of mixer intermodulation levels as function of local oscillator power level," *IEEE Trans. Electromagn. Compat.*, vol. EMC-13, pp. 56–63, May 1971.

[2] J. W. Graham and L. Ehrman, "Nonlinear systems modeling and analysis with applications to communications receivers," Rome Air Dev. Ctr. Tech. Rep. No. RADC-TR-73-178.

[3] J. H. Lepoff and A. M. Cowley, "Improved intermodulation rejection in mixers," *IEEE Trans. Microwave Theory Tech.*, vol. MTT-14, pp. 618–23, Dec. 1966.

[4] C. P. Tou and B. C. Chang, "A technique for intermodulation reduction in mixers" in *IEEE Symp. Electromagn. Compat., Dig. of Papers*, 1981, pp. 128–132.

[5] A. Ushida and L. O. Chua, "Frequency-domain analysis of nonlinear circuits driven by multi-tone signals," *IEEE Trans. Circuits Syst.*, vol. CAS-31, pp. 766–779, Sept. 1984.

[6] L. M. Orloff, "Intermodulation analysis of crystal mixer," *Proc. IEEE*, vol. 52, pp. 173–179, Feb. 1964.

[7] R. B. Swerdlow, "Analysis of intermodulation noise in frequency converters by Volterra series" *IEEE Trans. Microwave Theory Tech.*, vol. MTT-26, pp. 305–313, Apr. 1978.

[8] E. N. Gusinskiy, L. M. Kushnir, and N. V. Soina, "The level of intermodulation and combination interference in a diode mixer," *Telecommun. Radio Eng.*, vol. 32, no. 5, pp. 127–129, May 1977.

[9] L. M. Kushnir, V. V. Soina, M. S. Fogel'son, and E. N. Gusinskiy, "Influence of diode and load parameters on intermodulation noise suppression in a diode mixer," *Telecommun. Radio Eng.*, vol. 33, no. 3, pp. 118–120, Mar. 1978.

[10] J. G. Gardiner and A. M. Yousif, "Distortion performance of single-balanced diode modulators" *Proc. Inst. Elec. Eng.*, vol. 117, no. 8, pp. 1609–1614, Aug. 1970.

[11] D. N. Held and A. R. Kerr, "Conversion loss and noise of microwave and millimeter-wave mixers: Part 1-Theory; Part 2-Experiment" *IEEE Trans. Microwave Theory Tech.*, vol. MTT-26, pp. 49–61, Feb. 1978.

[12] S. A. Maas, *Microwave Mixers*. Dedham, MA: Artech House, 1986.

[13] A. R. Kerr, "A technique for determining the local oscillator waveforms in a microwave mixer," *IEEE Trans. Microwave Theory Tech.*, vol. MTT-23, pp. 828–831, Oct. 1975.

[14] Borland International, 4113 Scotts Valley Dr., Scotts Valley, CA 95066.

[15] S. Maas, "An interactive microwave mixer analysis program," Aerospace Corp. Technical Rep. No. TR-0086(692502)-8, 1986.

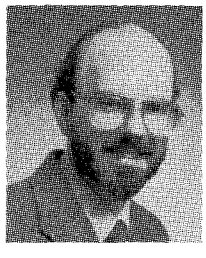

Stephen A. Maas (S'80–M'83) was born in Quincy, MA, in 1949. He received the B.S.E.E. and M.S.E.E. degrees in electrical engineering from the University of Pennsylvania in 1971 and 1972 and the Ph.D. degree in electrical engineering from the University of California, Los Angeles, in 1984.

He has been involved in research and development of low-noise and wide-dynamic-range receiving systems and components for radio astronomy and space communications at the National Radio Astronomy Observatory, Hughes Aircraft Company, and TRW. He is currently a Research Scientist at the Aerospace Corporation, with interests in FET/HEMT amplifiers, mixers, and intermodulation phenomena.

Dr. Maas is the author of *Microwave Mixers* (Artech House, 1986).